Investigation on Shock Induced Stripping Breakup Process of A Liquid Droplet

Yao Liu* , Ben Guan* and Chih-Yung Wen*

Department of Mechanical Engineering, The Hong Kong Polytechnic University, Hunghom, Kowloon, Hong Kong

Hua Shen†

Applied Mathematics and Computational Science, King Abdullah University of Science and Technology, Saudi Arabia

Abstract

Stripping breakup process of a single liquid droplet under the impact of a planar shock wave is investigated both experimentally and numerically. The droplet breakup experiment is conducted in a horizontal shock tube and the evolution of the droplet is recorded by direct high-speed photography. The experimental images clearly illustrate the droplet interface evolution features from its early to relatively late stage. Compressible Euler equations are solved using an in-house inviscid upwind characteristic space-time conservation element and solution element (CE/SE) method coupled with the HLLC approximate Riemann solver. A reduced five-equation model is employed to demonstrate the air/liquid interface. Numerical results accurately reproduce the water column and axi-symmetric water droplet breakup processes in experiments. The present study confirms the validity of the present numerical method in solving the shock wave induced droplet breakup problem and elaborates the stripping breakup process numerically in a long period. Droplet inner flow pattern is depicted, based on which the drives of protrusions emerged on the droplet surface are clearly seen. The droplet deformation is proved to be determined by not only the outer air flow, but also the inner liquid flow.

I. Introduction

The interaction of shock wave and an individual liquid droplet, yielding the consequent aerodynamic breakup of the droplet, poses a fundamental and challenging two-phase flow problem. The researches on this problem have been continued for decades in the aerospace and nuclear engineering communities due to its importance in the industrial applications, such as the ablation management of space vehicles caused by rain droplet impingement during an atmosphere reentry, supersonic combustion in multiphase mixtures for scramjet engines, and the damage evaluation and evacuation planning in case of a nuclear plant explosion, etc.

Traditionally, the types of liquid droplet breakup according to the value of the Weber number (We) can be classified into six modes:[1,2] vibrational mode, bag mode, bag-and-stamen mode, multi-wave piercing mode, stripping mode, and catastrophic mode. But Theofanous et al.[3–6] denied the catastrophic mode by experimental method. A smooth surface is observed at the windward stagnation area by their LIF (laser induced fluorescence) technique. Thus, the existence of Rayleigh-Taylor instability at the windward stagnation area is excluded. In addition, two new criticalities for the principal breakup modes are proposed by Theofanous et al., naming the Rayleigh-Taylor piercing (RTP) and shear-induced entrainment (SIE) corresponding to different We numbers. In supersonic flows, the stripping/SIE is the most universal breakup mode, however, the detailed breakup mechanisms and flow features of this mode are still not fully understood.

*Department of Mechanical Engineering, The Hong Kong Polytechnic University Hunghom, Kowloon, Hong Kong.

†Research associate, Applied Mathematics and Computational Science, King Abdullah University of Science and Technology, Saudi Arabia.

Focusing on the stripping mode, people conducted plenty of classical experiments in a variety of ways. Wierzba and Takayama[7] performed their shock tube experiments combined with five different photographic techniques and established the famous four-stage mechanism of the stripping type breakup. Hsiang and Faeth et al.[8–10] conducted a series of experiments concentrating on the atomization and spay problems and improved the famous droplet deformation and breakup regime map. Theofanous et al.[3–6] did plenty of excellent jobs in the aerodynamic breakup of liquid droplet in a rarefied supersonic flow using their LIF technique. They not only recorded clearly the droplet evolution, but also redefined the breakup mechanism. In order to minimize the uncertainty in visualizing the three dimensional shock/droplet interaction, two dimensional liquid columns are adopted. Igra and Takayama[11,12] performed experiments on shock/water-column interactions in a shock tube by sequential double-exposure holographic interferograms. Sembian et al.[13] successfully observed the propagation of waves inside the water column for incident Ma 1.75 and 2.4 by creating a water columns of 22 mm in diameter using super-hydrophobic coating technique.

Although the most fruitful achievements are obtained in experimental methods, the computational fluid dynamics played a significant role in understanding the droplet breakup mechanism. Various numerical works were performed in recent years. Based on their experimental results, Igra and Takayama[14] studied the shock/water column interaction using an interpolated pseudo-particle (CIP) scheme. Chen[15] reported 2D simulations of stripping breakup of a water column where the five-equation model was solved by a Godunov-type scheme coupled with the HLLC-Riemann solver. Theofanous et al.[6] combined the numerical code MuSiC$^+$ and AROS to simulate the droplet breakup process observed in their experiments. Where the MuSiC$^+$ code provides the shear stress distributions and viscous boundary layer details around a drop as input to AROS, and the AROS predicts viscous KH dispersion on the drop surface. Meng and Colonius[16,17] studied the effects of shock strength on the droplet breakup. The five-equation model was solved by a 3rd order WENO scheme coupled with the HLLC Riemann solver.

However, most of the existing studies are focused either on the first stage of droplet deformation or on the pure numerical validation. The outer air flow is consumed to be the only drive of the droplet deformation. It leads to incomplete understanding of the droplet breakup mechanism. As a result, a comprehensive experimental and numerical investigation is still needed. The purpose of the present study is to elucidate the stripping breakup mode of a single liquid droplet induced by a planar shock wave. Experimental and numerical results are combined to present the detailed deformation and breakup mechanism of liquid droplet.

II. Experimental and numerical methods

The experiments are conducted in a shock tube facility producing an incident shock with Ma number 1.52 with the post-shock density $\rho_g = 1.14$ kg·m^{-3} and post-shock velocity $u_g = 248.6$ m·s^{-1}. Water droplets with 2.5 mm in diameter D are used in the present study. Under this condition, the corresponding We number and Re number are:

$$We = \frac{\rho_g u_g^2 D}{\sigma} = 3.0 \times 10^3 \quad \text{and} \quad Re = \frac{\rho_g u_g D}{\mu_g} = 3.3 \times 10^4 \tag{1}$$

where σ is the surface tension and μ_g is the viscosity. Direct high-speed photography is employed to record the droplet breakup process. The sequential images have a resolution of 45 pixels/mm and exposure times as fast as 250 ns.

In the present study, the compressible Euler equations are solved using CE/SE method to simulate the shock/interface interaction. The volume fraction-based five-equation model is solved to illustrate the gas/liquid interface evolution, which can be expressed as:

$$\begin{aligned} &\tfrac{\partial \alpha_i}{\partial t} + V \cdot \nabla \alpha_i = 0, \quad i = 1, 2 \\ &\tfrac{\partial \rho_s \alpha_s}{\partial t} + \nabla \cdot (\rho_s \alpha_s V) = 0, \quad s = 1, 2 \\ &\tfrac{\partial \rho V}{\partial t} + \nabla \cdot (\rho V \otimes V + p) = 0 \\ &\tfrac{\partial E}{\partial t} + \nabla \cdot (V(E + p)) = 0 \end{aligned} \tag{2}$$

where the α_i denotes the volume fraction of fluid i, ρ_s the density of fluid s, ρ the density of the mixture, V the velocity vector, p the pressure and E the total energy.

The stiffened gas equation of state (EOS) is adopted to close the system:

$$p = (\gamma - 1)(E - \frac{1}{2}\rho V \cdot V) - \gamma\pi \tag{3}$$

where,

$$\frac{1}{\gamma-1}=\Sigma\frac{\alpha_i}{\gamma_i-1}\quad\text{and}\quad\frac{\gamma\pi}{\gamma-1}=\Sigma\frac{\alpha_i\gamma_i\pi_i}{\gamma_i-1} \tag{4}$$

The total density and the sound speed of the mixture can be respectively calculated as:

$$\rho=\Sigma\alpha_i\rho_i\quad\text{and}\quad c=\sqrt{\gamma(p+\pi)/\rho} \tag{5}$$

The five-equation model is solved using a maximum-principle satisfying upwind CE/SE scheme which was proved capable of capturing the contact interface without obvious diffusion.[18–20] HLLC approximate Riemann solver is employed to get the numerical fluxes between the conservation element. Validation of the numerical methods can be found in Shen et al.'s researches.[18–20] It is proved to be perfect in the numerical conservative properties in both space and time and accurate in capturing shock and contact discontinuities.

III. Results and analysis

The numerical method is first validated by simulating the shock/water-column interaction[13] (figure 1). The zero time is taken at the instant of shock impact and the dimentionless time t^* is defined as:

$$t^*=tu_g/D \tag{6}$$

Numerical density gradient (right-upper) and pressure distribution (right-lower) comparing with the experimental image (left) are presented at four distinct instants.

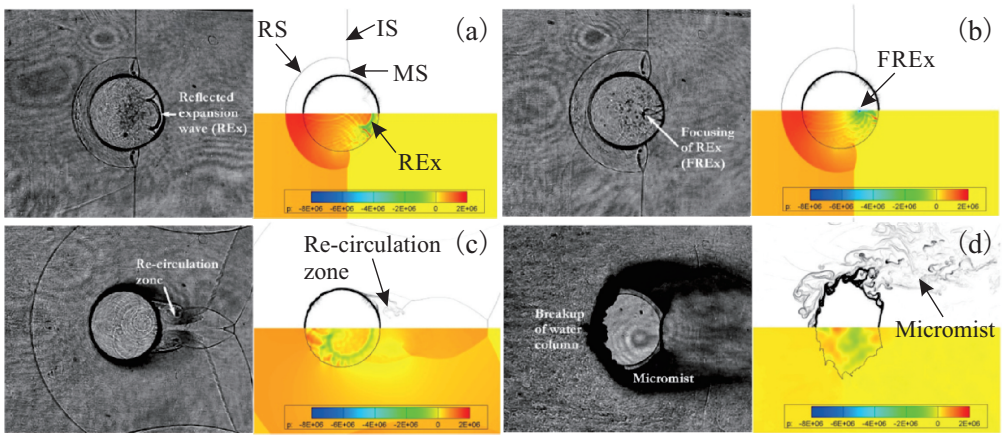

Figure 1. Sequential images of water column deformation and breakup for Mach 2.4 at t*=0.39 (a), 0.44 (b), 1.87 (c), 9.51 (d). The left shadow graphs of each sub-figures are experimental images of Sembian et al.,[13] the right upper half and lower half are numerical density gradient and pressure contour respectively.

The incident shock propagates from left to right and impinges the water column. At t^*=0.39, the incident shock (IS), reflected shock (RS) and the Mach stem (MS) intersect in a triple point, and the reflected expansion wave (REx) is clearly seen within the water column in figure 1(a). Due to the acoustic impedance mismatch between the air and water, waves propagate much faster in the water than that in air. The REx focuses at a single point (FREx) immediately at t^*=0.44 while the incident shock moves a very short distance in figure 1(b). After the passage of the incident shock, the flow field is built and a recirculation zone is formed at the leeward side of the water column at t^*=1.87 in figure 1(c). And finally, the water column breaks up in a striping mode as shown at t^*=9.51 in figure 1(d). Images illustrated in figure 1 validates the present numerical method in capturing both wave structures and contact interfaces. Thus, the following study can be proceeded based on the present method.

Figure 2 shows comparisons of sequential experimental images of a spherical drop deformation and breakup with shock Ma=1.52 and We=3000 and the corresponding numerical results. The comparisons are made in two ways, the lower half image in the upper row presents a 2D view where the simulation results represent a middle slice of the water droplet, and the lower half image in the lower row presents a 3D view where the air/droplet interface is represented by an iso-surface with water volume fraction 0.05. As shown

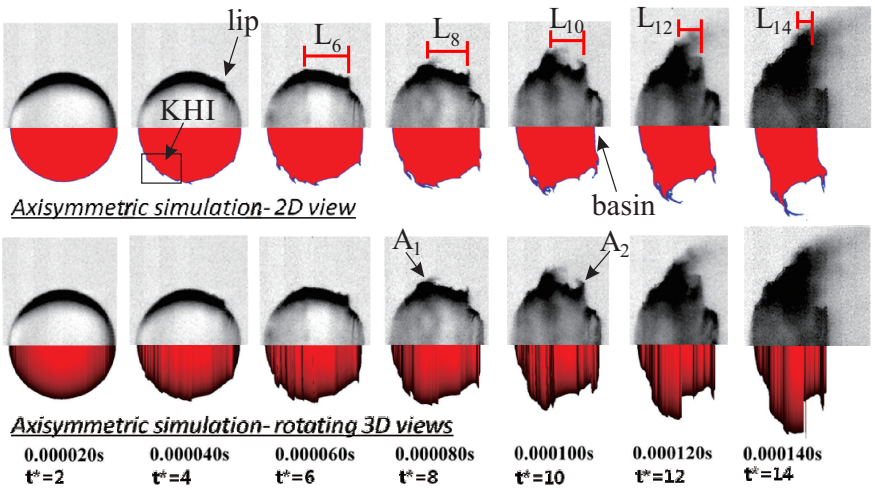

Figure 2. Sequential images of spherical drop deformation and breakup at Mach 1.52 and W_e=3000 and its comparison with the corresponding axisymmetric CE/SE simulation ($\alpha_{water} \geq$0.05).

in figure 2, the entire deformation and breakup process can be well simulated. In this case, the incident shock wave propagates from left to right and the starting time is defined as the instant when the incident shock wave impinges the liquid surface at the windward stagnation point. At $t^* = 2$, the incident shock wave passes the liquid droplet, and the flow field is initially established. At this early moment, the droplet can be deemed as a solid sphere where a perfect spherical form is maintained. At $t^* = 4$, the lip structure is formed at the leeward surface of the droplet as well as the shear induced ripples at the windward surface (marked as KHI which is caused by the Kelvin−Helmholtz instability). However, smooth surfaces are kept at both the windward and leeward stagnation areas. The size of lip and the shear induced ripples grow with time, and the width of the droplet in the transverse direction is compressed ($t^* = 6 \sim 14$, see also figure 3(a)). The mark of breakup occurs at $t^* = 8$ when atomization first happens at the protrusion near the droplet equator (denoted as A_1). The second atomization point occurs at the lip tip ($t^* = 10$, denoted as A_2), although the lip appears first. It is interesting to note that the atomized lip tip (A_2) is left pointing. As time elapse, the distance between the first atomization point (A_1) and the second atomization point (A_2) labeled as L becomes shorter, which is illustrated in the figure that $L_6 < L_8 < L_{10} < L_{12} < L_{14}$ where the subscripts denote the time. This indicates the flow direction at the left and right sides of the droplet are opposite. The opposite flow direction enhances the formation of the vortices at the lateral side which is benefit to the stripping breakup process. From the instant $t^* = 8$, a basin shaped leeward surface emerges and its depth increases. The interface evolution history is depicted in figure 3(a). The development of the basin depth leads to further droplet lateral growth, making the striping phenomenon even severer.

Figure 3(b) presents the vorticity distribution of the flow field at the early stage ($t = 20\mu$s). After the incident shock passage, the vorticity is produced mainly concentrating in a region near the droplet surface. At the windward side of the droplet, the vorticity distribution is confined on the droplet surface except the area near the stagnation point where the angle between the fluid flow and the surface normal direction is small. The separation occurs near the droplet equator (S). In this case, the vorticity acts as an index of flow direction. It shows that the air flow separates tangentially near the droplet equator. At the droplet windward surface out of the stagnation area, an interface protrusion occurs (KH), which is induced by the K-H instability. The vorticity at the leeward stagnation area is as weak as the windward stagnation area. However, the vorticity distribution between the separation point and the leeward stagnation point is complex and fascinating. In the inset of figure 3(b), the complex part of the vorticity is enlarged and streamlines are illustrated. The streamlines out of the separation region are regular ones while the streamlines in the separation region are twisted. In the separation region, three distinct vortices are formed, labelled as ω_1, ω_2 and ω_3 separately. This flow structure is in accordance with the researches of Theofanous et al.[6] and Meng et al.[16] The three vortices are rotating in different directions: ω_1 clockwise, ω_2 anti-clockwise and ω_3 clockwise. These vortices locate closely at the droplet surface and force the surface to deform. The surface area between ω_1 and ω_2 is pressed to "sink" into the droplet, while the surface area between ω_2 and ω_3 is "pulled up" into the air (deformation trend is depicted using red arrows). The clockwise rotating vortices ω_1

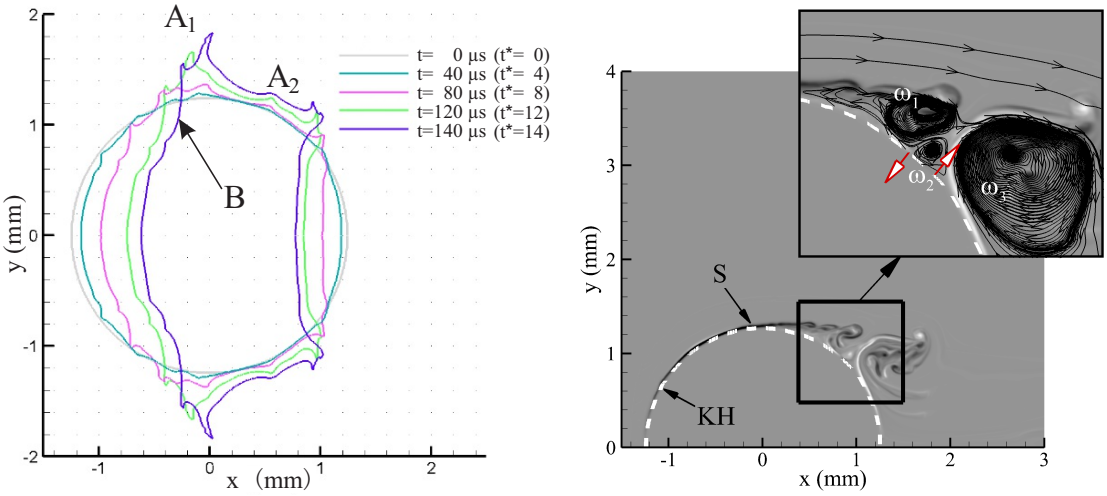

Figure 3. Deformation history of the water droplet surface by the CE/SE simulation (a) at Ms=1.52 and We=3000, and vortices distribution (b) at t=20 μs (t*=2) in Figure 2. S denotes the separation point, KH the area where the KH instability emerges. ω_1, ω_2 and ω_3 denotes three distinct vortices. The white dashed line represents the air/water interface (volume fraction of heavy fluid 95%). Light color indicates positive vorticity and dark color indicates negative vorticity.

and ω_3 are the reason why the protrusion A_2 atomization happens windward. And the distance decreasing between A_1 and A_2 can be well explained. Figure 3 shows that the outer air flow field of the shock/droplet interaction is built up in a very early stage. There is an obvious hysteresis of the droplet deformation after the flow field has been built up.

In the numerical results, the liquid protrusion in the middle of the leeward droplet surface is slightly weaker than the experimental images. The main reason is that the numerical code does not take the surface tension variation into account. As the shock wave passes by, the surface tension becomes smaller with the increase of gas temperature. In that case, the small liquid protrusion is easy to be extended into lips.

The inner flow of the water droplet in the shock/droplet interaction has seldom been considered in previous works because of its low flow speed. However, there is no doubt that the droplet deformation is a combined action of the inner and outer flow of the droplet. It is incomplete to only interpret the deformation from the perspective of outer flow. Figure 4 presents the inner flow field of the water droplet by illustrating the pressure distribution as well as the streamlines at a series of instants. When the incident shock impinges a spherical droplet, Mach stem emerges at the droplet surface and then it diffracts (DS) at the leeward surface, see (a), 5 μs. At this moment, the inner flow field has already been built up by the much faster transmitted shock. Streamlines shown within the droplet coincides with the precursory transmitted shock in the droplet. At instant (b) 7 μs, the inner flow basically remains intact, except the minor change affected by the diffracted shock (DS). At (c) 9 μs, the DS near the leeward stagnation point forms a high pressure zone, and re-diffracts to the windward. This high pressure zone is vital to the inner flow field. It produces a negative speed in the x direction, and a half saddle point (HS) is formed at the axis of symmetry. The windward-moving re-diffracted shock imposes direct disturbance only at the leeward stagnation area. The vortices formed near the leeward surface well "protect" the droplet surface from disturbance of any shock wave (d, 11 μs). After its formation, the half saddle point HS is moving windward until the moment (e), 20 μs. From 20 μs on, the location of HS is kept steady at approximately a fixed point (x =0.4$\sim$0.5 mm), and the droplet can be considered as two parts divided by the streamlines emitted from the HS point. It also should be noted that, up to this time (e, 20 μs), the droplet surface contour (the white solid line) is still maintained as a perfect circle. Also at this time, both the outer and inner flow field has been built up without the droplet deformation. A prediction of droplet deformation can be made based on the inner flow: there will be two protrusions emerging at the droplet surface, one is formed at the intersection of droplet surface and the streamlines emitted from the HS point (i.e. A_2), and the other one is formed at the leeward surface of the droplet surface near the largest vortex (i.e. A_3). Apparently, these two protrusions are formed via different mechanisms, A_2 is formed by the inner fluid flow driven by the high pressure zone at the leeward stagnation point, while A_3 is formed by the outer fluid flow driven by the vortex. The deformation at (f,

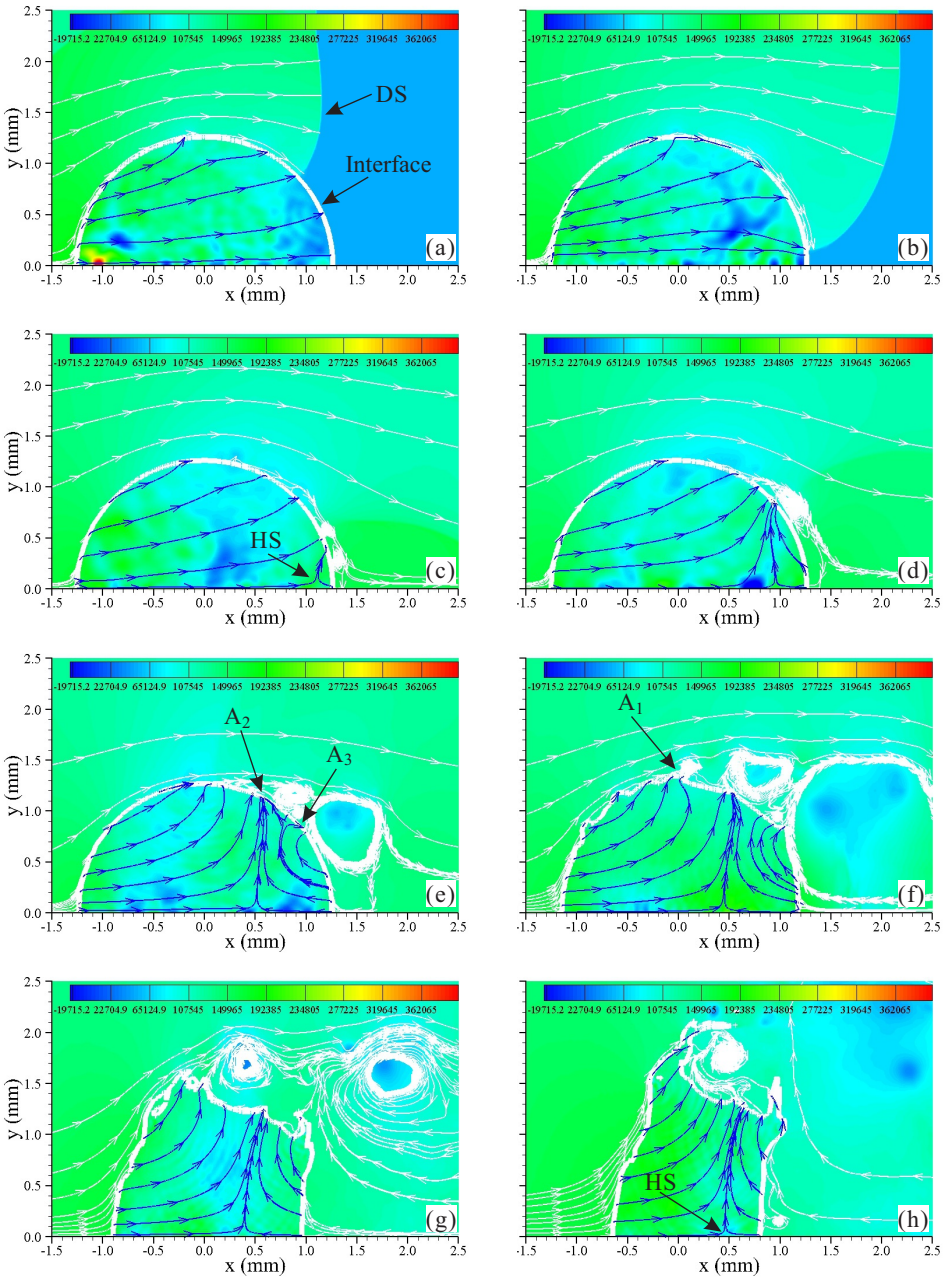

Figure 4. Numerical pressure distribution and streamlines at (a) 5 μs, (b) 7 μs, (c) 9 μs, (d) 11 μs, (e) 20 μs, (f) 50 μs, (g) 100 μs and (h) 140 μs. The white solid line denotes the air/water interface, DS the diffracted shock, Bif the bifurcated point.

50 μs) proves this prediction. Besides, the third protrusion (A_1) can be seen near the droplet equator at this moment, which is formed mainly by the outer low pressure zone. As time elapses, the droplet deforms obviously (g, 100 μs) in both the lateral and transverse directions, but the HS point keeps nearly still (h, 140 μs).

IV. Conclusion

Both experimental and numerical methods are employed to investigate the striping mode of a single water droplet. The experimental results are well simulated by the present numerical method. Details that can not be obtained from the experimental images are well captured in a numerical way. Different from the previous studies which focus on the outer flow field of a droplet, the present work takes both the inner and outer flow into account. By illustrating the inner flow streamlines, an interesting flow pattern is revealed. It is found that both the inner and outer flow field is built up at a very early time when the droplet is intact. The high pressure zone formed by the diffracted shock plays a fundamental role in building up the inner flow field. The most distinguishing feature of the inner flow is the half saddle point (HS). The streamlines emitted from the HS divide the droplet into two parts and lead to the forming of one of the protrusions on the droplet surface (i.e. A_2 or "the lip"). The location of HS keeps still since the building up of the whole flow field. In summary, a comprehensive perspective combining both the inner and outer flow field is expected to be more pertinent to understanding the stripping breakup process of liquid droplet.

Acknowledgments

This research was supported by the opening project of State Key Laboratory of Explosion Science and Technology (Beijing Institute of Technology), numbered KFJJ15-09M, Natural Science Foundation of China project, numbered 11372265, and the projects of Research Grants Council, Hong Kong, under contract number CRF C5010-14E and GRF 152151/16E.

References

[1]Pilch, M. and Erdman, C., "Use of breakup time data and velocity history data to predict the maximum size of stable fragments for acceleration-induced breakup of a liquid drop," *International journal of multiphase flow*, Vol. 13, No. 6, 1987, pp. 741–757.

[2]Joseph, D. D., Belanger, J., and Beavers, G., "Breakup of a liquid drop suddenly exposed to a high-speed airstream," *International Journal of Multiphase Flow*, Vol. 25, No. 6, 1999, pp. 1263–1303.

[3]Theofanous, T., Li, G., and Dinh, T.-N., "Aerobreakup in rarefied supersonic gas flows," *Journal of fluids engineering*, Vol. 126, No. 4, 2004, pp. 516–527.

[4]Theofanous, T. and Li, G., "On the physics of aerobreakup," *Physics of Fluids (1994-present)*, Vol. 20, No. 5, 2008, pp. 052103.

[5]Theofanous, T., "Aerobreakup of Newtonian and viscoelastic liquids," *Annual Review of Fluid Mechanics*, Vol. 43, 2011, pp. 661–690.

[6]Theofanous, T., Mitkin, V., Ng, C., Chang, C., Deng, X., and Sushchikh, S., "The physics of aerobreakup. II. Viscous liquids," *Physics of Fluids (1994-present)*, Vol. 24, No. 2, 2012, pp. 022104.

[7]Wierzba, A. and Takayama, K., "Experimental investigation of the aerodynamic breakup of liquid drops," *AIAA journal*, Vol. 26, No. 11, 1988, pp. 1329–1335.

[8]Hsiang, L.-P. and Faeth, G., "Near-limit drop deformation and secondary breakup," *International Journal of Multiphase Flow*, Vol. 18, No. 5, 1992, pp. 635–652.

[9]Hsiang, L.-P. and Faeth, G., "Near-limit drop deformation and secondary breakup," *International Journal of Multiphase Flow*, Vol. 18, No. 5, 1992, pp. 635–652.

[10]Faeth, G., Hsiang, L.-P., and Wu, P.-K., "Structure and breakup properties of sprays," *International Journal of Multiphase Flow*, Vol. 21, 1995, pp. 99–127.

[11]Igra, D. and Takayama, K., "A Study of Shock Wave Loading on a Cylindrical Water Column," *Reports of the Institute of Fluid Science, Tohoku University*, Vol. 13, 2001, pp. 19–36.

[12]Igra, D. and Takayama, K., "Experimental Investigation of Two Cylindrical Water Columns Subjected to Planar Shock Wave Loading," *Journal of Fluids Engineering*, Vol. 125, No. 2, 2003, pp. 325–331.

[13]Sembian, S., Liverts, M., Tillmark, N., and Apazidis, N., "Plane shock wave interaction with a cylindrical water column," *Physics of Fluids (1994-present)*, Vol. 28, No. 5, 2016, pp. 056102.

[14]Igra, D. and Takayama, K., "Numerical simulation of shock wave interaction with a water column," *Shock Waves*, Vol. 11, No. 3, 2001, pp. 219–228.

[15]Chen, H., "Two-dimensional simulation of stripping breakup of a water droplet," *Aiaa Journal*, Vol. 46, No. 5, 2008, pp. 1135–1143.

[16]Meng, J. and Colonius, T., "Numerical simulations of the early stages of high-speed droplet breakup," *Shock Waves*, Vol. 25, No. 4, 2015, pp. 399–414.

[17]Meng, J. C. and Colonius, T., "Droplet Breakup in High-Speed Gas Flows," *8th International Conference on Multiphase Flow*, May, 2013.

[18]Shen, H., Wen, C.-Y., and Zhang, D.-L., "A characteristic space–time conservation element and solution element method for conservation laws," *Journal of Computational Physics*, Vol. 288, 2015, pp. 101–118.

[19]Shen, H. and Wen, C.-Y., "A characteristic space–time conservation element and solution element method for conservation laws II. Multidimensional extension," *Journal of Computational Physics*, Vol. 305, 2016, pp. 775–792.

[20]Shen, H., Wen, C.-Y., Parsani, M., and Shu, C.-W., "Maximum-principle-satisfying space-time conservation element and solution element scheme applied to compressible multifluids," *Journal of Computational Physics*, Vol. 330, 2017, pp. 668–692.